Optimality considerations for propulsive fuselage power savings

Seitz, Arne; Luisa Habermann, Anaïs; van Sluis, Martijn

DOI
10.1177/0954410020916319

Publication date
2020

Document Version
Final published version

Published in
Proceedings of the Institution of Mechanical Engineers, Part G: Journal of Aerospace Engineering

Original Article

Institution of MECHANICAL ENGINEERS
Journal of AEROSPACE ENGINEERING

Proc IMechE Part G:
J Aerospace Engineering
0(0) 1–18

DOI: 10.1177/0954410020916319
journals.sagepub.com/home/pig
SAGE

Optimality considerations for propulsive fuselage power savings

Arne Seitz[1], Anaïs Luisa Habermann[1] and Martijn van Sluis[2]

Abstract

The paper discusses optimality constellations for the design of boundary layer ingesting propulsive fuselage concept aircraft under special consideration of different fuselage fan power train options. Therefore, a rigorous methodical approach for the evaluation of the power saving potentials of propulsive fuselage concept aircraft configurations is provided. Analytical formulation for the power-saving coefficient metric is introduced, and, the classic Breguet–Coffin range equation is extended for the analytical assessment of boundary layer ingesting aircraft fuel burn. The analytical formulation is applied to the identification of optimum propulsive fuselage concept power savings together with computational fluid dynamics numerical results of refined and optimised 2D aero-shapings of the bare propulsive fuselage concept configuration, i.e. fuselage body including the aft–fuselage boundary layer ingesting propulsive device, obtained during the European Union-funded DisPURSAL and CENTRELINE projects. A common heuristic for the boundary layer ingesting efficiency factor is derived from the best aero-shaping cases of both projects. Based thereon, propulsive fuselage concept aircraft design optimality is parametrically analysed against variations in fuselage fan power train efficiency, systems weight impact and fuselage-to-overall aircraft drag ratio in cruise. Optimum power split ratios between the fuselage fan and the underwing main fans are identified. The paper introduces and discusses all assumptions necessary in order to apply the presented evaluation approach. This includes an in-depth explanation of the adopted system efficiency definitions and drag/thrust bookkeeping standards.

Keywords

Boundary layer ingestion, fuel burn analysis, fuselage wake filling, mechanical power train, power-saving coefficient, propulsive fuselage aero-shaping, turbo-electric power train

Date received: 30 October 2019; accepted: 28 February 2020

Introduction

Novel propulsion systems and their synergistic integration with the airframe are expected to play a key role in pursuing aviation's challenging long-term sustainability targets. The recuperation of aircraft skin friction-induced flow momentum via Boundary Layer Ingesting (BLI) propulsion – the so-called wake-filling propulsion integration – is considered to be a technological enabler for strong improvements in overall vehicular propulsive efficiency. Long known from the field of marine propulsion, the positive effect of wake-filling on propulsive power requirements has been subject to theoretical treatise in aeronautics over several decades (e.g. Smith and Roberts,[1] Goldschmied,[2] Smith[3] and Drela[4]).

The most promising airframe component for wake-filling propulsion integration is the fuselage due to its large share of aircraft overall viscous drag. Initial experimental studies related to fuselage BLI and wake-filling were conducted for the boundary layer controlled airship body concept proposed by F.R. Goldschmied in 1957.[5] More recently, low-speed wind tunnel experiments were performed on a generic streamline body by ONERA[6] and TU Delft.[7] First experiments have also been performed at MIT for the D8 configuration.[8]

The most straightforward way of tapping the full fuselage wake-filling potential (360° installation) can be realised through a single BLI propulsor encirculating the fuselage aft body in addition to the underwing main engines, also known as propulsive fuselage concept (PFC).[9] While a first patent with explicit

[1]Bauhaus Luftfahrt e.V., Visionary Aircraft Concepts, Taufkirchen, Germany
[2]Department of Flight Performance and Propulsion, Technical University of Delft, Faculty of Aerospace Engineering, Delft, The Netherlands

Corresponding author:
Arne Seitz, Bauhaus Luftfahrt eV, Visionary Aircraft Concepts, Willy-Messerschmitt-Str. 1 Taufkirchen 82024, Germany.
Email: arne.seitz@bauhaus-luftfahrt.net

reference to fuselage wake-filling propulsion integration had already been filed in 1941,[10] various concepts on how to exploit the postulated benefits of fuselage wake-filling have been proposed in the most recent past. Proposed PFC aircraft configurations include NASA's 'FuseFan' concept,[11] the EADS/AGI 'VoltAir',[12] the Boeing 'SUGAR Freeze'[13] and the NASA 'STARC-ABL'.[14] Within the EU-FP7 project 'DisPURSAL',[15] a first multidisciplinary design study of PFC systems layout for large transport category aircraft was performed. During the ongoing EU-H2020 project 'CENTRELINE', the PFC proof-of-concept and initial experimental validation is pursued.[16]

Defining a PFC aircraft requires the best and balanced specification of a number of new top-level design parameters from the outset. Beside main design descriptors for size and positioning of the aft–fuselage BLI fan one of the most decisive design drivers is the fan power split between the non-BLI main engines and the BLI aft–fuselage propulsor. The purpose of the present paper is to provide guidance on the optimum choice of this key design parameter. Its optimal selection strongly depends on key system configurational and technological design decisions. Assuming an optimised aero-shaping, key influences are being exerted by the characteristics of the fuselage fan (FF) power train, i.e. the transmission efficiency and its specific weight, the performance of the main engines, as well as the aircraft application case, e.g. long range versus short range, and the overall systems design integration. Special consideration in the present paper will be paid to the impact of different FF power train options with regard to optimal power saving constellations for PFC aircraft design.

The effect of transmission efficiency on optimum PFC has been firstly evaluated by Gray and Martins[17] for NASA's STARC-ABL in a numerical optimisation study based on 2D axisymmetric computational fluid dynamics (CFD) simulation results. Their results showed that increasing efficiency of the FF power train has a significant effect on the optimum configuration: for an increased transmission efficiency the maximum achievable PSC increases and the optimum design moves to higher FF power shares.

The present paper introduces an analytical formulation approach to the evaluation of PFC power savings that allows for parametric analyses on optimum design trends for maximum power savings including aero-propulsive as well as basic system weights effects. As an aerodynamic basis, design and analysis results from the CENTRELINE and DisPURSAL projects are employed. In both projects, preliminary CFD simulation-based PFC aero-shaping and power train conceptual evaluation have been performed for a wide-body aircraft application scenario featuring a standard payload capacity of 340 passengers. The PFC aircraft configurations in both cases feature two underwing podded power plants supplemented by an aft–fuselage BLI fan. While in DisPURSAL an independent third gas turbine engine powered the FF, the CENTRELINE FF is powered through turbo-electric offtakes from the wing-mounted main engines. An electric FF drive alleviates many problems associated with the aero-structural integration of mechanically powered FFs.

Methodology

In the present paper, the cruise power-saving potentials of PFC aero-designs developed during DisPURSAL as well as preliminary design solutions from CENTRELINE are analysed and discussed with regard to optimality conditions. The basic PFC aircraft configuration considered features three propulsive devices – two conventional under wing podded power plants and an aft-fuselage BLI fan. The studied PFC designs cover broad ranges of key design parameters such as FF size, longitudinal positioning and design pressure ratio, as well as, the split between FF and overall fan shaft power. In this section, the methodological foundation for the analytical treatment is presented. All presented formulation focuses on high-speed steady level flight conditions, in the first instance.

System definition and bookkeeping of aerodynamic forces

Aerodynamic forces bookkeeping. In order to meaningfully compare the aerodynamic performance of wake-filling and conventional non-BLI aircraft, unified definition rules for the aerodynamic forces are required. Therefore, it is helpful in the first instance, to differentiate between those aircraft components immediately affected by BLI propulsion system integration and those with slightly less intensive aerodynamic coupling to the BLI propulsion system. In case of a PFC aircraft, the fuselage and the FF propulsion system are particularly tightly coupled. This bare PFC configuration can be distinguished from the adjacent aircraft components such as the wing, wing-podded engines and the empennage, provided aerodynamic interference is tracked appropriately.

The aerodynamic forces acting on the bare PFC configuration are defined according to the momentum conservation-based control volume approach proposed by Habermann et al.[18] The net propulsive force $NPF_{PFC,bare}$ is the total effective net force acting on the bare PFC configuration without interference from the residual aircraft components. It is defined as the difference between FF disc force $F_{disc,FF}$ and the sum of integrated viscous and pressure forces on the component surfaces $F_{PFC,bare}$

$$NPF_{PFC,bare} = F_{disc,FF} - F_{PFC,bare} \tag{1}$$

Specifically, $F_{PFC,bare}$ comprises the FF nacelle and fuselage aerodynamic forces. In contrast to $F_{PFC,bare}$,

the force acting on the overall aircraft $F_{PFC,tot}$ includes all aerodynamic forces acting on the components of the entire aircraft in clean configuration

$$F_{PFC,tot} = F_{PFC,bare} + F_{PFC,res} = F_{fus} + F_{FF,nac} + F_{res} \quad (2)$$

with the residual aerodynamic forces acting on all aircraft components other than the bare PFC configuration

$$F_{res} = F_{wing} + F_{nac} + F_{pyl} + F_{emp} \quad (3)$$

As indicated in Figure 1, the rearward acting surface forces pointing in drag direction (F_{wing}, F_{nac}, F_{emp}, F_{fus}, F_{pyl}, $F_{FF,nac}$) have a positive sign. Thrust forces ($F_{disc,FF}$, $F_{N,main}$, $NPF_{PFC,bare}$) are positive in accordance with MIDAP Study Group convention.[19]

The overall aircraft drag $D_{PFC,tot}$ is the sum of the forces acting on the components, the possible interference drag e.g. between the bare PFC and adjacent airframe components D_{int} as well as D_{misc}. The miscellaneous drag term includes drag due to protuberances and leakages, as well as the potential flow buoyancy terms of the individual components, which in sum become zero for the closed aircraft body

$$\begin{aligned} D_{PFC,tot} &= F_{PFC,bare} + F_{PFC,res} + D_{PFC,int} + D_{PFC,misc} \\ &= F_{PFC,bare} + D_{PFC,res} \end{aligned} \quad (4)$$

The interference drag includes drag due to interference of all aircraft components, including interference at the wing–fuselage junction as well as the intersection of fuselage, vertical tail plane, and FF nacelle in front of and inside the FF inlet. A more detailed discussion of this is presented in Baseline parametric settings section.

For a non-BLI reference aircraft, the total drag is defined analogously with $F_{FF,nac} = 0$ yielding

$$\begin{aligned} D_{Ref,tot} &= F_{Ref,fus} + F_{Ref,res} + D_{Ref,int} + D_{Ref,misc} \\ &= D_{Ref,fus} + D_{Ref,res} \end{aligned} \quad (5)$$

Main engine efficiency figures:

Definition of power plant overall efficiency: For fuel-powered aircraft, power plant overall efficiency is defined by the ratio of effective propulsive power P_{thrust} to the power supplied to the combustion chamber via fuel enthalpy flow P_{supply} (cf. e.g. Seitz et al.[20])

$$\eta_{ov} = \frac{P_{thrust}}{P_{supply}} = \frac{V_0 \cdot F_N}{\dot{m}_f \cdot FHV} \quad (6)$$

where V_0 represents the flight velocity and F_N denotes the streamtube net thrust. The fuel enthalpy flow is expressed in terms of the fuel mass flow $\dot{m}_f$ and its lower heating value FHV. Power plant overall efficiency may be conveniently split into the product of the core, transmission and propulsive efficiencies

$$\eta_{ov} = \eta_{co} \cdot \eta_{tr} \cdot \eta_{pr} \quad (7)$$

The propulsive efficiency η_{pr} captures the dissipative losses in the flow field of the propulsive jet. For ducted propulsive devices this means the ratio of P_{thrust} and the power in the jet at the nozzle exit P_{jet}.[a] The core efficiency η_{co} in a gas turbine engine accounts for the high pressure (HP) system including upstream effects of the core mass flow, such as the inner streamtube, intake and ducting losses, as well as, polytropic compression in the fan and low pressure compressor. η_{co} describes the ratio between the ideal power $P_{co,id}$ at the core engine exit plane CE that is available for the low-pressure turbine (LPT) to drive the outer fan, i.e. the part of the fan working on the bypass mass flow, and, P_{supply}. It can be expressed as (cf. Kurzke[21])

$$\eta_{co} = \frac{P_{co,id}}{P_{supply}} = \frac{\dot{m}_{co} \cdot \left(\Delta h_{is,CE\rightarrow amb} - \frac{V_0^2}{2}\right)}{\dot{m}_f \cdot FHV} \quad (8)$$

where $P_{co,id}$ is determined by the core engine mass flow $\dot{m}_{co}$ and the theoretical delta enthalpy available from isentropic expansion from core exit conditions to ambient pressure $\Delta h_{is,CE\rightarrow amb}$, i.e. after all power requirements (e.g. compression processes) of the core stream are satisfied. As a transitory item, the free-stream kinetic energy of $\dot{m}_{co}$ when entering the control volume of η_{co} is not accounted for in the η_{co} definition, and thus, subtracted from the product of $\dot{m}_{co}$ and Δh_{is} to yield $P_{co,id}$. The transmission efficiency η_{tr} relates the power in the propulsive jet P_{jet} to $P_{co,id}$.

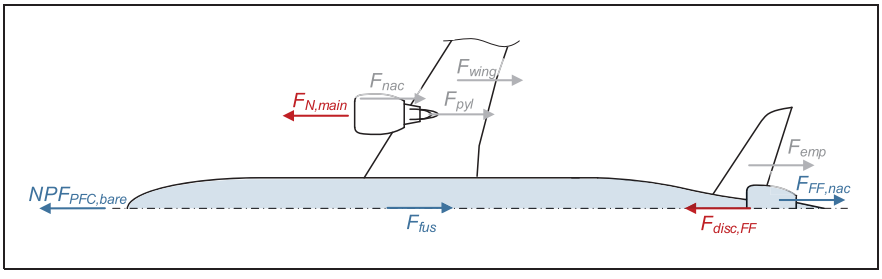

Figure 1. Bottom view of PFC aircraft with cruise aerodynamically acting force annotated and bare PFC configuration highlighted in blue.

In the case of a turbofan engine, the control volume of η_{tr} comprises the LPT, the core nozzle, the low-pressure (LP) shaft including optional reduction gearbox system, the fan, as well as all internal losses associated with the propulsive device, i.e. outer streamtube, intake, bypass ducting and nozzle losses. The individual control volumes of η_{co}, η_{tr} and η_{pr} are indicated in Figure 2.

Aero-numerical analysis and shape optimisation approach

The aerodynamic data basis of the present analysis is formed by 2D-axisymmetric Reynolds Averaged Navier Stokes (RANS) CFD simulation results of the bare PFC configuration, i.e. the simplified fuselage body including the aft–fuselage propulsion system for typical cruise conditions at zero angle of attack. Simulations within DisPURSAL were performed on multi-block structured meshes with ONERA's CFD software 'elsA'[22] using the Spalart–Allmaras turbulence model. FFs were emulated using actuator disk boundary conditions based on the Glauert theory.[23]

The external aerodynamics of the PFC within the CENTRELINE project are evaluated using the commercial software package ANSYS Fluent® (Version 18.2). The axisymmetric pressure-coupled solver is used to exploit the fact that the PFC design is axisymmetric, reducing the computational cost considerably. Due to the importance of the state of the boundary layer for the overall system performance, the boundary layer is resolved up to the wall and the $k-\omega$ shear stress transport turbulence model is used. Other turbulence models, such as the one-equation model by Spalart–Allmaras or the $k-\omega$ Reynolds Stress Model, were also tested for comparison but did not yield significantly different results.

A higher order scheme (Monotonic Upwind Scheme for Conservation Laws, MUSCL[24]) is used for the spatial discretisation of the momentum and energy equation. Turbulence quantities are discretised using the Quadratic Upstream Interpolation for Convective Kinematics (QUICK) scheme.[25] The fluid is treated as an ideal gas with a non-constant specific heat and viscosity modelled with Sutherland's three-coefficient method.

The fluid domain is a C-grid with the boundaries placed at least 10 fuselage lengths away from the body. The upstream, upper and downstream boundaries are treated as a pressure far-field boundary condition, meaning that the free-stream Mach number, temperature and static pressure at infinity are prescribed. The far-field boundary condition is a non-reflecting condition based on the Riemann invariants. The fuselage and the nacelle are modelled as an adiabatic no-slip wall. The mesh is constructed using ANSYS ICEM® and consists solely of hexahedron mesh elements. The mesh resolution near the walls is set such that $Y^+ < 1$ is guaranteed everywhere on the body surface. A limited mesh dependency study was performed to ensure mesh independency. The analysis showed that a mesh size of approximately 350,000–400,000 cells yields a refined enough mesh to effectively eliminate errors dependent directly on the grid.

To model the FF, a simple body-force method is applied. In the mesh, a separate fluid domain is defined which represents the box volume around the fan. In Fluent, a momentum density (N/m^3) source term is added to all cells within the domain containing the fan. The source term is incorporated in the momentum equation as an external body force $\vec{F}$. Since only axial momentum is added and no swirl component is accounted for, the modelling of the stator is not taken into account in the preliminary aerodynamic CFD model. Due to flow compressibility, energy needs to be added to the flow to ensure an increase in total enthalpy of the fluid. Thus, sources of energy (J/m^3) are added to account for the work done by the fan. In this case, only axial momentum is added, and hence the energy term can simply be computed by

$$\epsilon = \overrightarrow{F_a} \cdot V_a \tag{9}$$

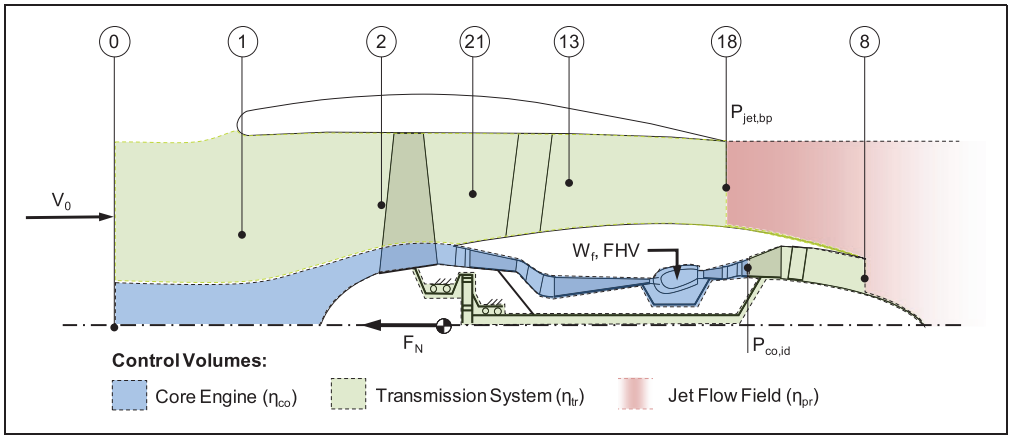

Figure 2. Control volume definition for podded power plant system installation including thermodynamic station designation.

where ϵ is the energy source, $\overrightarrow{F_a}$ the axial external force by the fan and V_a the local axial velocity component. Integration of the energy source over the volume directly yields the power added to the fluid by the FF. Similarly, the total addition of momentum density integrated over the mesh volume representing the fan yields the total force added.

The design parameter for the FF is the fan pressure ratio (FPR), which is defined as the ratio between the mass-averaged total pressures upstream and downstream of the fan.

As a means of validation for the fuselage modelling in CFD, a direct comparison was conducted between the RANS results based on the source model and typical propulsion system performance modelling. For this purpose, Bauhaus Luftfahrt's in-house software Aircraft Propulsion System Simulation (APSS)[26–29] was employed. The geometric settings such as flow areas were directly adopted from the contour shaping. The intake total pressure recovery ratio compared to freestream conditions (p_2/p_0) was adjusted according to the RANS results. As can be seen from equation (1), the FF disk force constitutes an important quantity in the bookkeeping scheme. Assuming the disk to be thin, this parameter was calculated in APSS from the following momentum balance across the disc

$$F_{disc,FF} = \dot{m}_{FF}\left(V_{FF,out} - V_{FF,in}\right) + \left(p_{s,FF,out} - p_{s,FF,in}\right) \cdot A_{disc,FF} \tag{10}$$

where $\dot{m}$ refers to the mass flow, V to the axial flow velocity, p_s to the static pressure and A_{disc} to the flow annulus area at the FF actuator disc position. The isentropic fan power $\left(P_{sht,FF,is} = \dot{m} \cdot \Delta h_{is,FF}\right)$ was compared to the fan power obtained from the CFD calculation. The agreement of both models in terms of FF performance prediction was found to be good, with a deviation in disk force and ideal shaft power of less than 2%. In order to cross-validate the CFD modelling performed in DisPURSAL and CENTRELINE, a representative PFC aero-shaping case was analysed in both aero-numerical setups. It was found that the mapping of bare PFC drag forces and FF disc power absorptions was in very good agreement, as deviations in results stayed clearly below 2%. The predicted FF disc forces, however, deviated by approximately 5%. As a most likely reason for this, the different types of models for the FF actuator disc were identified, yielding for example deviations of approximately 2% in FF mass flow for identical FF pressure ratios.

For the performance assessment of BLI/wake-filling propulsion system concepts such as the CENTRELINE and DisPURSAL PFC configurations, an overview of applicable figures of merit is provided by Habermann et al.[18] As a means of aerodynamic inter-comparison of alternative PFC designs and optimisation criterion during aerodynamic shape refinement, in the present context, the bare PFC efficiency factor, $f_{\eta,PFC,bare}$, is used

$$f_{\eta,PFC,bare} = \frac{NPF_{PFC,bare} \cdot V_0}{P_{disc,FF}} \quad \left\{P_{disc,FF} | P_{disc,FF} > 0\right\} \tag{11}$$

This metric relates the net useful propulsive power, i.e. the product of the net axial propulsive force acting on the bare PFC configuration $NPF_{PFC,bare}$ and the flight velocity V_0 to the ideal power expended in the FF disc, $P_{disc,FF}$.

Analytical formulation of power and fuel savings

Evaluation of power-saving coefficient. For the comparative assessment of PFC designs against the non-wake-filling reference aircraft configuration, the power-saving coefficient *PSC* originally introduced by Smith[3] is used

$$PSC = \frac{P_{Ref} - P_{PFC}}{P_{Ref}} \tag{12}$$

where P_{Ref} refers to the power required to operate the aircraft in the conventional, non-BLI case, and, P_{PFC} represents the power requirements of the PFC configuration. For the evaluation of the *PSC* metric it is reasonable to initially focus on the aero-propulsive integration effects of BLI propulsion, and, to assume conventionally podded gas turbines as main power plants. This allows for a *PSC* determination without the consideration of gas turbine cycle (i.e. η_{co}) implications, in the first instance. With this focus, it is convenient to compare the effective core engine excess powers $P_{co,eff}$ for the BLI and non-BLI case when assessing the *PSC*.

$P_{co,eff}$ includes the free shaft power extracted from the LPT in order to drive the propulsor[b] $P_{co,sht}$ and the residual excess power in the core flow at the LPT exit (Station 5) $P_{co,res}$

$$P_{co,eff} = P_{co,sht} + P_{co,res} \tag{13}$$

With $P_{co,sht}$ and $P_{co,res}$ expressed thermodynamically

$$P_{co,sht} = \dot{m}_{co} \cdot \Delta h_{LPT,free} = \frac{P_{Fan,o}}{\eta_{mech,LP}} = \frac{\dot{m}_{bp} \cdot \Delta h_{F,o}}{\eta_{mech,LP}} \tag{14}$$

$$P_{co,res} = \dot{m}_{co} \cdot \left(\Delta h_{is,5\rightarrow amb} - \frac{V_0^2}{2}\right) \tag{15}$$

where $\Delta h_{LPT,free}$ denotes the effective specific free work of the LPT and $\Delta h_{Fan,o}$ is the effective specific work of the outer fan. The term $\Delta h_{is,5\rightarrow amb}$ represents the ideal residual work remaining after the turbine expansion process. The core and bypass mass flows are indicated by $\dot{m}_{co}$ and $\dot{m}_{bp}$, respectively,

while $\eta_{mech,LP}$ denotes the low pressure spool mechanical efficiency.

The effective core engine excess power $P_{co,eff}$ can be directly related to the ideal core engine excess power $P_{co,id}$ referred to in the core efficiency definition (cf. System definition and bookkeeping of aerodynamic forces section)

$$P_{co,eff} = f_{\eta,co,id\rightarrow eff} \cdot P_{co,id} \tag{16}$$

where the efficiency factor $f_{\eta,co,id\rightarrow eff}$ is a function of the LPT isentropic efficiency and the ratio of $P_{co,sht}$ and $P_{co,res}$. It is worthwhile to note that for a fixed thermodynamic cycle, i.e. invariant specific thrust levels of the core and bypass nozzles as well as constant η_{co} and η_{tr}, $f_{\eta,co,id\rightarrow eff}$ is a constant.

For non-BLI propulsive devices, the effective core engine exit power can be related to effective propulsive power P_{thrust} by the effective propulsive device efficiency $\eta_{pd,eff}$

$$\eta_{pd,eff} = \frac{V_0 \cdot F_N}{P_{co,eff}} \tag{17}$$

With equation (17), the required effective core engine exit power for the non-BLI reference aircraft $P_{co,eff,Ref}$ yields

$$P_{co,eff,Ref} = \frac{V_0 \cdot F_{N,Ref}}{\eta_{pd,eff,Ref}} \tag{18}$$

The required effective core engine exit power for the PFC aircraft results from the summation of the effective core engine exit powers for the non-BLI main engines $P_{co,eff,main}$ and the LPT shaft power required to drive the BLI FF $P_{co,sht,FF}$

$$P_{co,eff,PFC} = P_{co,eff,main} + P_{co,sht,FF} \tag{19}$$

where $P_{co,eff,main}$ can be determined using equation (17) as

$$P_{co,eff,main} = \frac{V_0 \cdot F_{N,main}}{\eta_{pd,eff,main}} \tag{20}$$

and $P_{co,sht,FF}$ directly results from the ideal power absorbed by the FF rotor disc $P_{disc,FF}$

$$P_{co,eff,FF} = \frac{P_{sht,FF}}{\eta_{PT,FF}} = \frac{P_{disc,FF}}{\eta_{PT,FF} \cdot \eta_{pol,FF}} \tag{21}$$

with the FF power train efficiency $\eta_{PT,FF}$ translating the delivered LPT shaft power to FF shaft power. The FF polytropic efficiency $\eta_{pol,FF}$ relates the shaft power absorbed by the FF $P_{sht,FF}$ to the power imparted on the air flow in the fan plane $P_{disc,FF}$. In the specific case of turbo-electric power transmission $\eta_{PT,FF,TE}$ equals the product of the cooled electric generator, motor and power management and distribution (PMAD) system efficiencies, η_{Gen}, η_{Mot} and η_{Mot}

$$\eta_{PT,FF,TE} = \eta_{Gen} \cdot \eta_{PMAD} \cdot \eta_{Mot} \tag{22}$$

Knowing appropriate values for the various efficiency figures, the computation of the $P_{co,eff}$ values for the reference and PFC aircraft as well as the subsequent PSC evaluation requires the determination of the respective propulsion system thrust demands. Assuming steady level flight, in the first instance, the total reference net thrust requirement for the non-BLI reference aircraft $F_{N,Ref}$ equals its total aerodynamic drag $D_{Ref,tot}$, expressed by the fuselage drag $D_{Ref,fus}$ and the overall aircraft residual drag $D_{Ref,res}$ including all aircraft viscous, pressure and induced drag components other than fuselage drag acc. to equation (3)

$$F_{N,Ref} = D_{Ref,tot} = F_{Ref,fus} + D_{Ref,res} \tag{23}$$

Analogously, for PFC aircraft, the overall net thrust $F_{N,PFC}$ needs to balance the PFC aircraft total drag $D_{tot,PFC}$

$$F_{N,PFC} = D_{PFC,tot} = F_{PFC,bare} + D_{PFC,res} \tag{24}$$

where the total aerodynamic force acting on the bare PFC configuration $F_{PFC,bare}$ is catered for by the fuselage BLI propulsive device and included in net propulsive force of the bare PFC configuration $NPF_{PFC,bare}$ (cf. equation (1)). The total net thrust requirement for the non-BLI power plants $F_{N,main}$ accordingly yields

$$F_{N,main} = D_{PFC,res} - NPF_{PFC,bare} \tag{25}$$

$NPF_{PFC,bare}$ can be calculated for a given $P_{disc,FF}$ using the definition of the bare PFC efficiency factor $f_{\eta,PFC,bare}$ (equation (11))

$$NPF_{PFC,bare} = \frac{P_{disc,FF} \cdot f_{\eta,PFC,bare}}{V_0} \tag{26}$$

Combining equations (25) and (26) with equation (19), the required effective core engine excess power for the PFC aircraft case can be analytically expressed as

$$P_{co,eff,PFC} = \frac{V_0 \cdot D_{PFC,res}}{\eta_{pd,eff,main}} + P_{disc,FF} \cdot \left(\frac{1}{\eta_{PT,FF} \cdot \eta_{pol,FF}} - \frac{f_{\eta,PFC,bare}}{\eta_{pd,eff,main}} \right) \tag{27}$$

Assuming identical efficiencies for the non-BLI propulsive devices of the PFC and reference aircraft, i.e. $\eta_{pd,eff,main} = \eta_{pd,eff,Ref} = \eta_{pd,eff}$, and, aircraft residual drags,[c] i.e. $D_{PFC,res} = D_{Ref,res} = D_{res}$, the PSC for

steady level flight can be formulated as follows

$$PSC = 1 - \left(\frac{D_{res}}{D_{Ref,tot}} + \frac{P_{disc,FF}}{V_0 \cdot D_{Ref,tot}} \cdot \left(\frac{\eta_{pd,eff}}{\eta_{PT,FF} \cdot \eta_{pol,FF}} - f_{\eta,PFC,bare} \right) \right) \tag{28}$$

Equation (28) includes four basic terms presenting key aspects for PFC design optimality:

- $D_{res}/D_{Ref,tot}$ is driven by the share of fuselage drag within the total drag balance of the non-BLI reference aircraft. It can be seen that for a growing fuselage drag share, the PSC metric is increasing.
- $P_{disc,FF}/\left(V_0 \cdot D_{Ref,tot}\right)$ relates the ideal power expanded in the FF to the overall thrust power required for the non-BLI reference aircraft. It is apparent, that this ratio is an important descriptor for the overall PFC aircraft design.
- $\eta_{pd,eff}/\left(\eta_{PT,FF} \cdot \eta_{pol,FF}\right)$ incorporates all transmission losses starting from the effective core engines excess power. When reducing losses in the FF power train, i.e. improved $\eta_{PT,FF}$ or $\eta_{pol,FF}$, PSC increases. Reducing the losses in the non-BLI propulsive device, i.e. improved $\eta_{pd,eff}$, reduces the PSC value.
- The BLI efficiency factor $f_{\eta,PFC,bare}$ expresses the net propulsive effect achieved by a certain power expanded at the FF disc. It is a direct representation of the aero-propulsive design of the bare PFC configuration at a given level of ideal FF power.

Evaluation of fuel savings. It should be noted that the PSC metric can also be assessed at the overall propulsion efficiency level by including η_{co} and $f_{\eta,co,id\rightarrow eff}$ in the evaluation. In this case, the powers P_{Ref} and P_{PFC} compared by the PSC refer to the powers supplied to both aircraft via fuel enthalpy flows ($P_{supply} = FHV \cdot \dot{m}_f$, cf. equation (6)). Assuming identical fuel types used for both aircraft, BLI and non-BLI, the PSC metric is equivalent to the reduction in instantaneous fuel flow rate $\dot{m}_f$ due to the BLI configuration at any given operating point

$$PSC = \frac{\dot{m}_{f,Ref} - \dot{m}_{f,PFC}}{\dot{m}_{f,Ref}} \tag{29}$$

With the PSC metric available in terms of fuel flow rates, it can be directly used for an initial evaluation of PFC aircraft fuel consumption. The Breguet–Coffin equation in integral form solved for consumed fuel mass m_f as a function of aircraft instantaneous gross weight $m_{A/C,end}$ at the end of a considered range segment ΔR serves as a basis for this

$$m_f = m_{A/C,end} \cdot \left(e^{\frac{\Delta R \cdot g}{FHV \cdot \eta_{ov} \cdot L/D}} - 1 \right) \tag{30}$$

where L/D and η_{ov} indicate the aircraft aerodynamic and the propulsion system overall efficiency values at a representative operating condition along ΔR, e.g. at $\Delta R/2$. Assuming steady level flight, i.e. $F_N = D_{tot}$, the required supply power P_{supply} at the representative operating point can be written as

$$P_{supply} = \frac{V_0 \cdot m_{A/C} \cdot g}{\eta_{ov} \cdot L/D} \tag{31}$$

Solving equation (31) for the BLI PFC and the non-BLI reference aircraft while considering $P_{PFC} = P_{Ref} \cdot (1 - PSC)$ according to equation (12) yields a direct relation between the vehicular efficiency numbers $\eta_{ov} \cdot L/D$ of the PFC and reference aircraft

$$(\eta_{ov} \cdot L/D)_{PFC} = \frac{(\eta_{ov} \cdot L/D)_{Ref}}{(1 - PSC)} \cdot \vartheta \tag{32}$$

where ϑ represents the ratio of instantaneous gross weights $m_{A/C}$ between the PFC and the reference aircraft at the considered representative cruise condition

$$\vartheta = \frac{m_{A/C,PFC}}{m_{A/C,Ref}} \tag{33}$$

When assessing the performance of PFC aircraft against non-BLI aircraft, both the pure PSC and the ratio of aircraft gross weights are significant. While vehicular efficiency quantification (equation (32)) necessitates an instantaneous ϑ at the considered operating point, the evaluation of fuel burn based on the solution of the Breguet–Coffin equation presented in equation (30) requires aircraft gross weight to be determined at the end of ΔR. Hence, equation (32) can be used to solve equation (30) for both aircraft and to analytically express the consumed fuel mass of the PFC aircraft $\Delta m_{f,PFC}$ for a given range segment ΔR as a function of the determined PSC, the vehicular efficiency of the reference aircraft $(\eta_{ov} \cdot L/D)_{Ref}$ as well as the aircraft gross weight ratios at the representative operating point and at the end of range segment, ϑ and ϑ_{end}

$$m_{f,PFC} = m_{A/C,Ref,end} \cdot \vartheta_{end} \cdot \left(e^{\frac{\Delta R \cdot g}{FHV \cdot (\eta_{ov} \cdot L/D)_{Ref}} \frac{(1-PSC)}{\vartheta}} - 1 \right) \tag{34}$$

It can be seen that for $PSC = 0$ and $\vartheta = \vartheta_{end} = 1$, i.e. the reference aircraft case, equation (34) is identical to the solution of the Breguet–Coffin formula presented in equation (30). The influence of PSC on BLI fuel savings is displayed in Figure 3. The trends show the increasing amplification of vehicular efficiency when translated to fuel burn as range is increased. At a theoretical range value $\Delta R = 0$nmi, PFC fuel savings equal the value of the PSC metric.

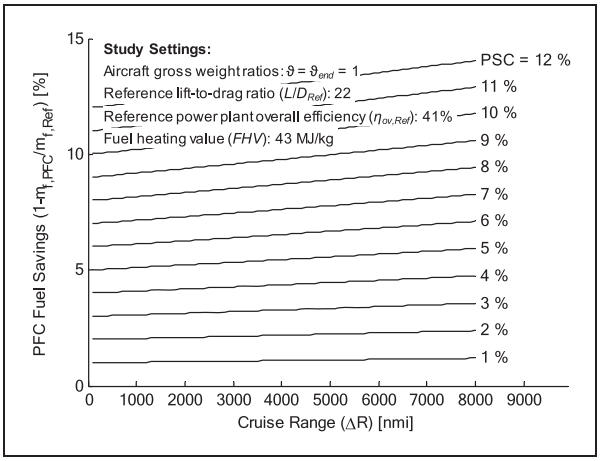

Figure 3. PSC impact on PFC fuel savings versus cruise range.

The PSC value for an actual PFC design can be obtained from equation (28), if PFC and reference aircraft share identical η_{co} and $f_{\eta,co,id\rightarrow eff}$. The aircraft gross weight ratio ϑ can be determined based on the absolute change in aircraft instantaneous gross weight $\Delta m_{A/C}$ – when changing from the non-BLI reference to the PFC configuration

$$\Delta m_{A/C} = \Delta m_{PG} + \Delta m_{OWE,Res} + \Delta m_{PL} + \Delta m_f \tag{35}$$

or expressed in relative terms (cf. equation (33))

$$\vartheta = \frac{m_{A/C,Ref} + \Delta m_{A/C}}{m_{A/C,Ref}} = 1 + \frac{\Delta m_{PG}}{m_{A/C,Ref}} + \frac{\Delta m_{OWE,Res}}{m_{A/C,Ref}} + \frac{\Delta m_{PL}}{m_{A/C,Ref}} + \frac{\Delta m_f}{m_{A/C,Ref}} \tag{36}$$

For a given transport task, the change in payload mass Δm_{PL} between reference and PFC aircraft will be zero. Considering an end-of-(cruise)-flight condition for ϑ_{end}, the residual fuel masses on both aircraft, PFC and reference, will be small, hence, the absolute fuel mass difference Δm_f will be small. Assuming Δm_f to be negligible for ϑ_{end}, $\Delta m_{A/C}$ can be determined from changes in structural, systems and equipment weights, summarised by the $\Delta m_{OWE,Res}$ term, as well as the weight changes in the propulsion group Δm_{PG}

$$\Delta m_{PG} = m_{PG,PFC} - m_{PG,Ref} \tag{37}$$

The weights of the propulsion groups in both aircraft cases (PFC and Ref) may be simply determined based on the weights of its principal component groups

$$m_{PG} = m_{PD} + m_{BTE} + m_{TM} + m_{ACC} \tag{38}$$

where the propulsive device group PD includes the fan, nacelle and nozzle weights, the bare turbo engine group BTE covers all turbo components and engine structures, the accessories group ACC spans all auxiliary systems and buyer furnished equipment, and, the transmission system TM captures the shaft and drive gear system of the non-BLI fans $m_{PT,main}$ as well as FF power train including thermal management in the PFC case $m_{PT,FF}$. For the present study purposes, each of those weight items is determined through simple scaling based on representative specific power values P/W (cf. also Aircraft application case section)

$$m_{PD} = \frac{P_{co,eff,tot}}{P/W_{PD}} \quad m_{BTE} = \frac{P_{co,eff,tot}}{P/W_{BTE}} \quad m_{ACC} = \frac{P_{co,eff,tot}}{P/W_{ACC}}$$
$$m_{TM} = \frac{P_{co,eff,main}}{P/W_{PT,main}} + \frac{P_{co,eff,FF}}{P/W_{PT,FF}} \tag{39}$$

where the individually significant shares of the total effective core engine excess powers are used as scaling parameters. The difference in residual aircraft operating empty weight $\Delta m_{OWE,Res}$ includes all aircraft structural and systems weight changes and the associated design cascade effects at aircraft level. The meaningful determination of $\Delta m_{OWE,Res}$ therefore would require an aircraft integrated sizing loop which is not part of the present scope. Instead, the effect of $\Delta m_{OWE,Res}$ will be discussed as a scenario parameter within the optimality analyses presented in Study results section.

While the assumption of $\Delta m_f = 0$ for the determination of ϑ_{end} is fair, Δm_f will be non-zero for representative cruise conditions as soon as $PSC \neq 0$, especially considering large values of ΔR. Therefore, the prediction of ϑ in equations (32) and (34) requires the identification of Δm_f e.g. midway through ΔR. Despite the fact that an accurate determination of Δm_f, here, would require an iterative solution, the correlation $\Delta m_f = m_{f,Ref} \cdot PSC$ is proposed an initial estimate for the calculation of ϑ.

Setup of study

Aircraft application case

The present study is performed based on the data and knowledge gained during the DisPURSAL and CENTRELINE projects up to the present point in time. Relevant top-level properties characterising the air transport tasks focused on in both projects are listed in Table 1.

The advanced DisPURSAL and CENTRELINE reference aircraft, both dubbed R2035, feature identical payload capacities of 340 passengers in a standard two-class cabin layout and are equipped with advanced aerodynamic, structural, systems and propulsion technologies to reflect a possible entry-into-service year 2035. While the outer dimensions of both aircraft are almost identical, the design

Table 1. Top-level aircraft properties for the DisPURSAL and CENTRELINE reference aircraft.

	DisPURSAL[15]	CENTRELINE[16]
Basic aircraft top-level requirements		
Technology freeze/entry-into-service	2030/2035	2030/2035
Design range	4800 nmi	6500 nmi
Design payload	340 PAX (2-class)	340 PAX (2-class)
Reference aircraft key properties		
Wing span	65.0 m	65.0 m
Fuselage length	67.0 m	66.7 m
Fuselage diameter	6.09 m	6.09 m
Operating empty weight	123.5 t	120.2 t
Maximum take-off weight	206.3 t	222.9 t
Design block fuel vs. year 2000 state-of-the-art	–32%	–27%

Table 2. Cruise drag properties and propulsion efficiency figures representative for CENTRELINE R2035 aircraft (cf. also Peter et al.30).

Drag properties[a] (kN)	
$D_{Ref,fus}$	24.7
$D_{Ref,res}$	67.7
$D_{Ref,tot}$	92.4
L/D_{Ref}	22.0
Power plant efficiency figures[a] (–)	
$\eta_{ov,Ref}$	0.41
$\eta_{co,Ref}$	0.58
$\eta_{tr,Ref}$	0.82
$\eta_{pr,Ref}$	0.87
$\eta_{pol,F,o}$	0.94
$f_{\eta,co,id\rightarrow eff}$	0.96
$\eta_{pd,eff,Ref}$	0.74

[a]Cruise at M0.82, FL350, ISA + 10 K; $c_L = 0.5$.

range of the R2035 in CENTRELINE features an increased design range of 6500 nmi versus the 4800 nmi of the DisPURSAL R2035. Alongside with the increased design range, the maximum take-off weight of the CENTRELINE R2035 is relatively increased by 8%. Both aircraft comply with ICAO Annex 14 Code E standards and feature fuel burn savings in the order of 30% compared to a year 2000 standard. While taking into account the PFC design configurations developed in both projects, the analyses presented later on in this paper will refer mainly to the CENTRELINE air transport case. Therefore, key properties relevant vehicular efficiency determination are presented for the CENTRELINE R2035 aircraft in Table 2.

For the investigation of weight impacts of the attainable PFC power and fuel savings specific powers for the principle component groups derived from the CENTRELINE R2035 propulsion group[30] are presented in Table 3.

Table 3. Specific powers for the principle component groups of the CENTRELINE R2035 propulsion system acc. to Samuelsson et al.[31]

Component group	Specific power (kW/kg)[a]
Propulsive device	2.92
Bare turbo engine	7.33
Accessories	37.8
Transmission system (main)	32.8

[a] w.r.t. $P_{co,eff}$ at typical cruise point.

Baseline parametric settings

Beyond the reference aircraft application scenario, the analysis of the PFC power-saving potentials requires a few assumptions to be made and motivated. These refer to the aerodynamic interference of the bare PFC configuration and the adjacent aircraft components, i.e. the lifting surfaces and the under wing podded power plants, as well as the efficiency of power transmission from the core engine exit to the FF, and the degradation of the FF efficiency itself due to the ingestion of distorted inflow.

Typical sources of aerodynamic interference would be caused by the 3D flow at the wing–fuselage junction and the intersection of the fuselage and FF nacelle body with the empennage, especially in flight with incidence (pitch and yaw[d]). While the aerodynamic inference between the wing and the fuselage at the fuselage–wing junction may be expected to be similar for best and balanced reference and PFC aircraft designs, for the empennage, configurations need to be considered that avoid aerodynamic interference with the FF nacelle as much as possible. Assuming a T-tail arrangement for the PFC configuration, the aerodynamic interference between the horizontal stabiliser and the bare PFC configuration is clearly reduced. The aerodynamic interference of the vertical

fin and the FF nacelle remains in this case. More advanced solutions such as self-trimming wing configurations[31] might allow for significant size reductions or possibly the total omission of tail planes. The data basis of CFD aerodynamic results used for the present study is limited to 2D axisymmetric simulations of the bare PFC configuration. All residual drag components from adjacent aircraft components are retained invariant when changing from the non-BLI reference to the BLI PFC aircraft. This means, aerodynamic interference effects between the bare PFC configuration and the rest of the aircraft are not explicitly resolved, in the first instance. At the same time, reduction drag effects due to shrinking main engine nacelle sizes for the PFC aircraft[e] as well as the ingested wake momentum deficits emanating from the wing and tail plane root sections are not accounted for.

The wake fields of upstream aircraft components have a direct impact on the inflow distortion of the aft–fuselage BLI propulsor. The main effects include the wing downwash, fuselage upwash at non-zero incidence as well as the tail plane wakes. By interfering with the fuselage boundary layer flow these wake effects create additional distortion in the BLI propulsor inflow field through circumferential asymmetry, thereby impacting of the aerodynamic efficiency of the FF. The reduction of BLI fan aerodynamic efficiency $\eta_{pol,FF}$ relative to fans operating under freestream inflow conditions has been previously investigated numerically and experimentally for various inflow distortion patterns. Gunn and Hall indicate an efficiency penalty between 1% and 2% for BLI fans in semi-buried engines configurations on the topside of a blended wing body aircraft.[32] Initial aerodynamic design and performance results for a FF propulsor under axisymmetrically distorted inflow have been produced as part of the CENTRELINE project by Castillo Pardo and Hall.[33] Relative to an optimised freestream inflow design Castillo Pardo and Hall predict a FF isentropic efficiency penalty between 0.5% and 1.0%. Based on an outer fan polytropic efficiency of the CENTRELINE reference power plants of $\eta_{pol,F,o} = 94\%$ this suggests a FF polytropic efficiency of $\eta_{pol,FF} = 93\%$.

The FF power train efficiency $\eta_{PT,FF}$ strongly depends of the transmission paradigm, which can be by electric, mechanical or pneumatic means. The considered options primarily considered in this study are turbo-electric, i.e. an electrically driven FF powered by generator off-takes from the main engines, and mechanical, i.e. via shaft and gearbox systems. An achievable turbo-electric power train efficiency based on conventional conducting, non-cyrogenic electric components typically is of the order of 90%, while all high temperature superconducting designs may be much closer to 100%. A mechanical transmission through a shaft and bearing system similar to a geared turbo fan engines possibly supplemented by two serial gear stages may be estimated at an efficiency of 98%. The core engine efficiencies η_{co} have been set identical for the BLI PFC and non-BLI reference aircraft, in the first instance. All studied cases use a FHV of 43 MJ/kg.

The focus of the present study is on steady-level flight at cruise conditions featuring a fuselage angle of attack of zero. With the 2D axisymmetric aerodynamic simulations, the analysis refers to aft-fuselage designs without upsweep. It should be noted that in reality, aft–fuselage upsweep will be a multi-disciplinary optimisation parameter trading aerodynamic penalties in terms of aft–fuselage pressure drag and FF performance penalties due to aerodynamic upwash effects, and structural weights reductions for example through relieved main landing gear length requirements during take-off rotation.

Study results

Aerodynamic shape refinement and optimisation

During DisPURSAL, an initial 2D axisymmetric aero-shaping for the bare PFC configuration based on semi-empirically derived design settings for FF size and pressure ratio[34] was iteratively refined based on a multi-disciplinary aircraft design exercise featuring CFD in-the-loop.[35] Starting from the refined baseline aero-shape, an initial CFD-based design space exploration was performed for alternative FF sizes and pressure ratios.[36] In the succeeding CENTRELINE project, a preliminary draft of the fuselage and FF nacelle aerodynamic geometry was generated based on previous design experience from DisPURSAL. The general fuselage dimensions, such as total fuselage length and diameter, were adopted from the CENTRELINE R2035 aircraft (cf. Peter et al.[37]). Based on preliminary design space analyses,[16] FF FPR was initially selected to be 1.40 and $P_{disc,FF}$ was constrained to 5.5 MW. Different from the FF aero-structural integration in DisPURSAL with the FF air intake located in front of the empennage, the geometric baseline in CENTRELINE assumed the FF to be far aft located along the fuselage central axis. The initial 2D axisymmetric shaping of the bare PFC configuration was incrementally improved based on engineering judgement and evaluated in CFD in order to maximise its aerodynamic efficiency. Modifications included nacelle incidence angle and aft body curvature improvements as well as increased fuselage boat tail length and the introduction of a gradual increase in hub diameter towards the exit of the duct, similar to those observed in state-of-the-art turbofan designs. An example of two different designs and their respective surface pressure distributions is shown in Figure 4.

As can be observed from the figure, the hub line of the fuselage near the duct exit is contracting much more in the case of the updated intermediate revision of the bare PFC design. In this way, the circumferential surface area is reduced and local surface normal vectors are

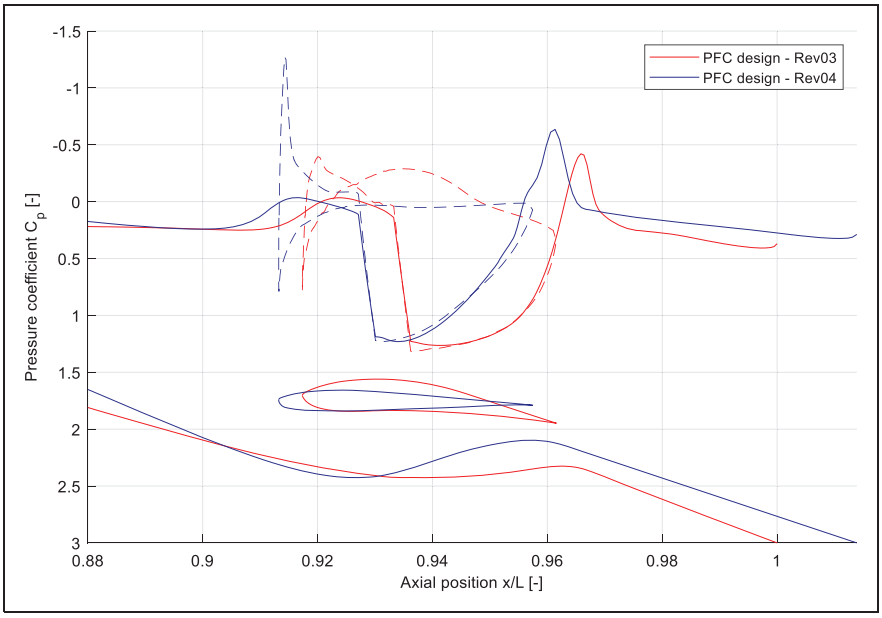

Figure 4. Comparison of the static pressure coefficient distribution of representative aero-shaping versions (Rev03 and Rev04) in cruise conditions (FL350, M0.82, ISA+10 K; $FPR_{FF} = 1.40$).

better aligned, to reduce the pressure drag on the nacelle. Furthermore, it allows for a less cambered nacelle geometry at lower incidence angle for a given duct exit area. The contraction of the hub line at the fan location also helps to prevent flow separation at the hub due to the contraction of stream tube. Additionally, the length of the fuselage boat tail was increased, to increase the positive axial force on the body due the higher static pressure in the exhaust plume of the FF.

In order to achieve a step-change improvement in PFC aero-shaping beyond the intuitive refinement approach, a numerical optimisation process based on a parametric model of the axisymmetric PFC geometry was developed. Therefore, the fuselage geometry was represented by various non-uniform rational basis (NURB) splines, to allow for local changes in curvature and shape. The nacelle geometry was replicated using the Bezier–Parsec method.[38] In total, 23 parameters were required to represent the full bare PFC configuration. An automated framework was created around the CFD setup discussed in Aero-numerical analysis and shape optimisation approach section in order to perform the entire procedure from geometry creation to meshing, and from simulation to data post-processing. A quasi-random sampling approach (Latinised Partial Stratified Sampling[39]) was used to cover the large sampling space. With a mesh to simulation convergence success rate of close to 40%, over 2000 converged unique results were obtained. One-dimensional sensitivity studies were conducted to identify the most influential design parameters. The key parameters determined for the shape optimisation were the following:

- Freestream Mach number (M_0)
- Flight altitude (h_0)
- FF pressure ratio (FPR_{FF})
- FF duct height (h_2)
- FF nozzle exit to fan front face area ratio (A_{18}/A_2)
- FF hub-to-tip ratio (r_{FF}/R_{FF})
- FF relative axial position along the fuselage (x_{FF}/L_{fus})

Using these parameters, a surrogate model based on support vector machines[40] was constructed. A survey of the sample space revealed several promising designs, of which one design was selected as being most suitable for the CENTRELINE configuration. Taking the selected design as a starting point, a constrained gradient-based optimisation was carried out to obtain best bare PFC aero-shapings with regard to the $f_{\eta,PFC,bare}$ metric. For the CENTRELINE design cruise conditions (FL350, M0.82 ISA + 10 K) and a given $P_{disc,FF}$ constraint of 5.5 MW, the aerodynamic optimum was found at design settings of $FPR_{FF} = 1.32$, $h_2 = 0.73$ m, $A_{18}/A_2 = 0.68$, $r_{FF}/R_{FF} = 0.43$ and $x_{FF}/L_{fus} = 0.92$.

The progression of aerodynamic efficiency with each revision of the CENTRELINE bare PFC aero-shaping is presented in Figure 5 including Rev 06 obtained from the abovementioned numeric optimisation process. As can be seen from the figure, the actual shaping of Rev 06 does not deviate drastically from the initial PFC designs (cf. Figure 4). However, the combined effect of relatively small changes to the aft body curvature, nacelle incidence and duct height of the FF, leads to clear performance improvements measurable by the bare PFC net propulsive power for the given level of $P_{disc,FF}$.

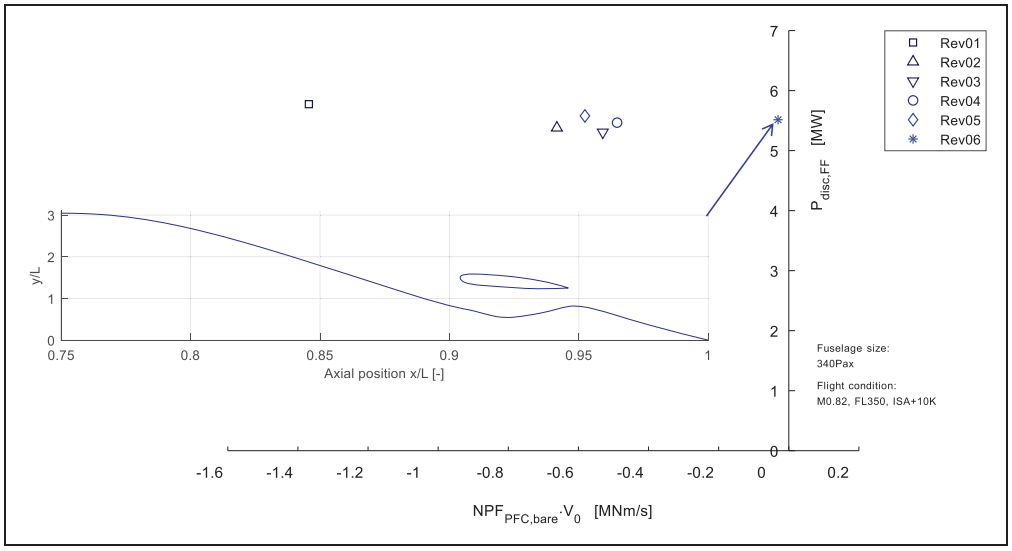

Figure 5. Progression of aerodynamic efficiency during CENTRELINE bare PFC aero-shape refinement with design contour after optimisation of the main shape parameters.

Analysis of aircraft power savings

In order to study optimality trends for PFC power savings, the entirety of PFC 2D aero-shaping cases evaluated in DisPURSAL and during CENTRELINE so far was taken into account. For this purpose, the studied aero-shaping cases were analysed with regard to the BLI efficiency factor for the bare PFC configurations (cf. equation (11)). A chart of $f_{\eta,PFC,bare}$ values for all designs plotted against the corresponding ideal powers absorbed by the FF discs is presented in Figure 6.

The shown bare PFC designs cover a wide range of $P_{disc,FF}$. Below approximately 6 MW, the BLI efficiency factor $f_{\eta,PFC,bare}$ is negative due to a negative $NPF_{PFC,bare}$. Hence, in this region the FF disc force $F_{disc,FF}$ is not sufficient to fully compensate the total retarding force acting on the bare PFC configuration. For increasing $P_{disc,FF}$ it can be seen that the BLI efficiency factor $f_{\eta,PFC,bare}$ improves strongly in the low-power region while the improvement trend flattens out towards the higher power region. As $P_{disc,FF}$ increases, the corresponding optimum FF face area grows as fan pressure ratio is limited for propulsive efficiency reasons. With growing face area the FF blade heights increasingly grow into the outer regions of the boundary layer profile where the local momentum deficit decreases rapidly. As such, the additionally ingested momentum deficit is reduced and the further gains from BLI are diminishing.

Given the power train design paradigms mainly followed in both projects, the CENTRELINE designs cover mostly the lower $P_{disc,FF}$ region while the DisPURSAL designs predominantly capture the high-power region. However, the best cases of both domains of bare PFC 2D aero-shaping consistently form a Pareto front with regard to $f_{\eta,PFC,bare}$. This allows for the determination of a high-quality data fitting curve for the designs the form that convex hull of the pool of designs

$$f_{\eta,PFC,bare} = 0.6919 - 12.4267 \cdot \left(P_{disc,FF}[MW] + 0.7687\right)^{-1.5481} \quad (40)$$

The validity of the above fitting correlation applies to 340 passenger wide body aircraft with design cruise conditions at around M0.82, FL350 ISA + 10 K and covers $P_{disc,FF}$ between approximately 2 and 26 MW. The correlation can be immediately used as a design heuristic in order to analytically compute the *PSC* according to equation (28). Validation plots for the PSC mapping quality based on equation (40) are presented in Figure 7, showing that an evaluation of equation (28) using the $f_{\eta,PFC,bare}$ fitting curve yields very good agreement – both in absolute values and in general trending behaviour – with a direct *PSC* evaluation based of the actual CFD data produced by ONERA and TU Delft during DisPURSAL and CENTRELINE, respectively.

The plots in Figure 7 display the best bare PFC aero-shapings from CENTRELINE and DisPURSAL indicated as convex hull points in the previous figure. For the design cases, two scenarios of FF power train efficiency $\eta_{PT,FF}$ are visualised – an ideal one featuring $\eta_{PT,FF} = 100\%$ and a more conservative one with $\eta_{PT,FF} = 90\%$. The obtained *PSC* values are plotted against the relative FF power, i.e. the ratio of ideal power absorbed by the FF disc to the total effective core engine excess power required for the PFC aircraft $P_{disc,FF}/P_{co,eff,tot}$. The relative FF power is one of the most basic and crucial design parameters to be selected at a very early stage of *PFC* aircraft conceptualisation. Therefore, Figure 7 offers

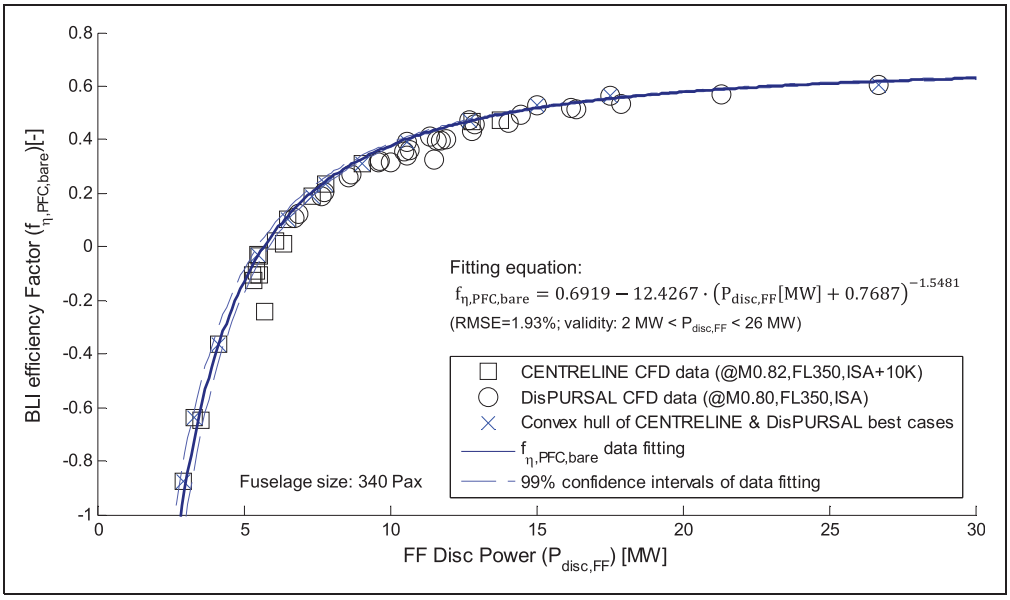

Figure 6. Analysis of BLI efficiency factor for CENTRELINE and DisPURSAL aero-shapings.

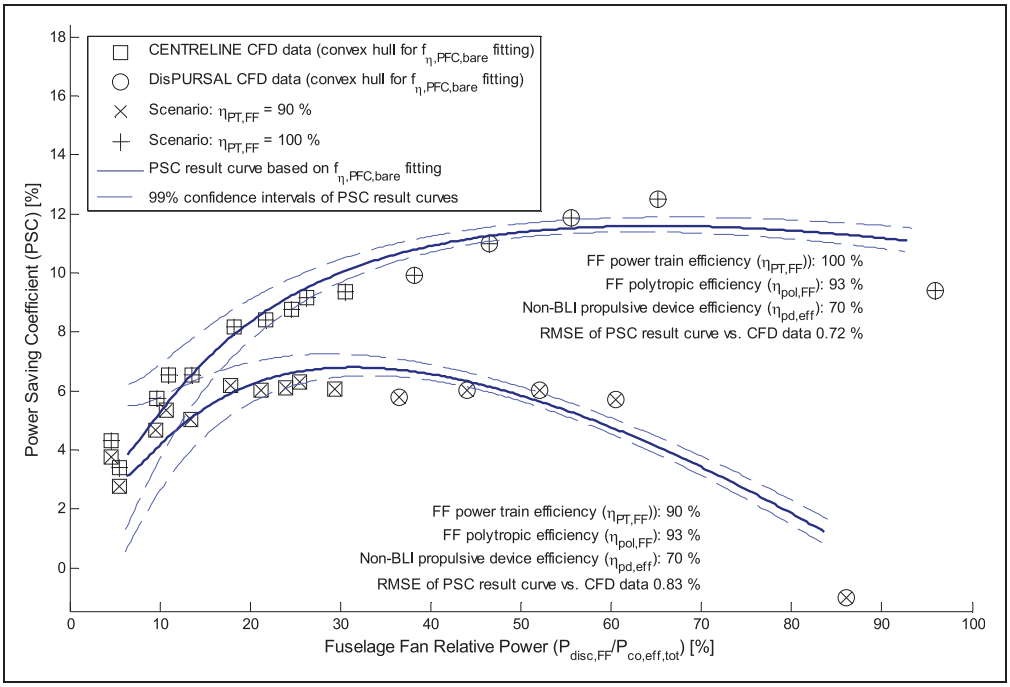

Figure 7. Analysis of PSC for CENTRELINE and DisPURSAL best aero-design cases.

clear indication of how to choose $P_{disc.FF}/P_{co,eff,tot}$ in order to obtain maximum PFC power savings. It can be seen from the figure that not only the achievable maximum *PSC* is reduced as more losses occur in the FF power train (cp. the clusters featuring $\eta_{PT,FF}$ of 90% and 100% in the figure), but also that the corresponding optimum $P_{disc.FF}/P_{co,eff,tot}$ shifts to lower values, meaning macroscopic changes to the entire PFC aircraft. Similar trends for varying FF transmission efficiency have been previously observed for a single-aisle aircraft application by Gray and Martins based on numerically optimised designs using 2D axisymmetric CFD simulation of the fuselage and FF nacelle body.[17] The common trending behaviours demonstrate how the balance of overall propulsive efficiency gains due to BLI and the associated adverse effects such as bare PFC retarding force for maximum *PSC* is influenced by the level of BLI propulsion system internal losses. It is worthwhile to note, however, that noticeable power savings can even be found at sub-optimally small $P_{disc.FF}/P_{co,eff,tot}$ designs where the $f_{\eta,PFC,bare}$ yields negative values.

Constellations for optimum power savings

In order to systematically gauge the sensitivity of optimum PFC power savings and corresponding aircraft design impact, parametric analyses of *PSC* (cf. equation (28)) based on the presented $f_{\eta,PFC,bare}$ fitting were performed. Optimum results with regard to the maximum PSC and corresponding $P_{disc.FF}/P_{co,eff,tot}$ are presented in Figure 8.

Figure 8 quantifies the importance of high FF transmission efficiencies $\eta_{PT,FF}$ in order to achieve significant *PSC* values. Comparing, for instance, a turbo-electric power transmission featuring $\eta_{PT,FF}=$ 91% and a mechanical power train with $\eta_{PT,FF}=$ 98% assuming $\eta_{pd.eff.non\text{-}BLI}=70\%$,[f] the maximum PSC for the mechanical case would yield 10.4% while maximum PSC for the turbo-electric case would be reduced by 3.3% down to a value of 7.1%. The corresponding optimum $P_{disc.FF}/P_{co,eff,tot}$ would be 55% for the mechanical case and reduced to 33% in the turbo-electric case since the larger transmission losses make the shift of power to the aft-fuselage BLI propulsor less attractive for maximum vehicular efficiency.

Beyond the pure sensitivity of maximum PSC and optimum design due to variations in $\eta_{PT,FF}$, Figure 8 also shows strong impact of the effective efficiency of the involved non-BLI propulsive devices – i.e. the reference and the PFC main engines $\eta_{pd.eff.non\text{-}BLI}$ – on optimum PFC design and the attainable power savings. Increasing $\eta_{pd.eff.non\text{-}BLI}$ raises the benchmark level for BLI propulsion, and thus, reduces the achievable PSC for a given level of $\eta_{PT,FF}$. At the same time, the optimum for FF relative power is decreased, indicating more power to be directed to the main engine propulsive devices. For the above defined turbo-electric and mechanical FF power transmission scenario cases, an increase in $\eta_{pd.eff.non\text{-}BLI}$ from 70% to 80% yields a reduction in maximum *PSC* by 3.9% and 5.2%, respectively.

Despite its insightful nature with regard to the vehicular efficiency of PFC aircraft, the PSC metric does not account for effects of changes in aircraft empty weight due the novel type of propulsion system and its airframe integration. Also, the effect of weight reduction due to varying fuel consumption along a given flight distance is not captured. Therefore, Figure 9 presents the PFC fuel burn savings based on the modified Breguet–Coffin equation (equation (34)) for a 340 passenger, 6500 nmi air transport task.

The optimum PFC fuel savings in Figure 9 are plotted against $\eta_{PT,FF}$. The specific power of the FF power train $P/W_{PT,FF}$ is shown as an array parameter. The ratio of aircraft gross weights between the PFC and reference aircraft design at the end of the considered flight segment ϑ_{end} is displayed as dash-dotted contours in blue colour. Optimum PFC design is indicated as solid contours of $P_{disc.FF}/P_{co,eff,tot}$ in green colour, while the correspondingly attainable *PSC* levels are represented as dotted contours in red colour. All study settings comply with the data defined in Tables 2 and 3.

The PFC fuel improvement trends versus increasing $\eta_{PT,FF}$ shown in Figure 9 are consistent with the

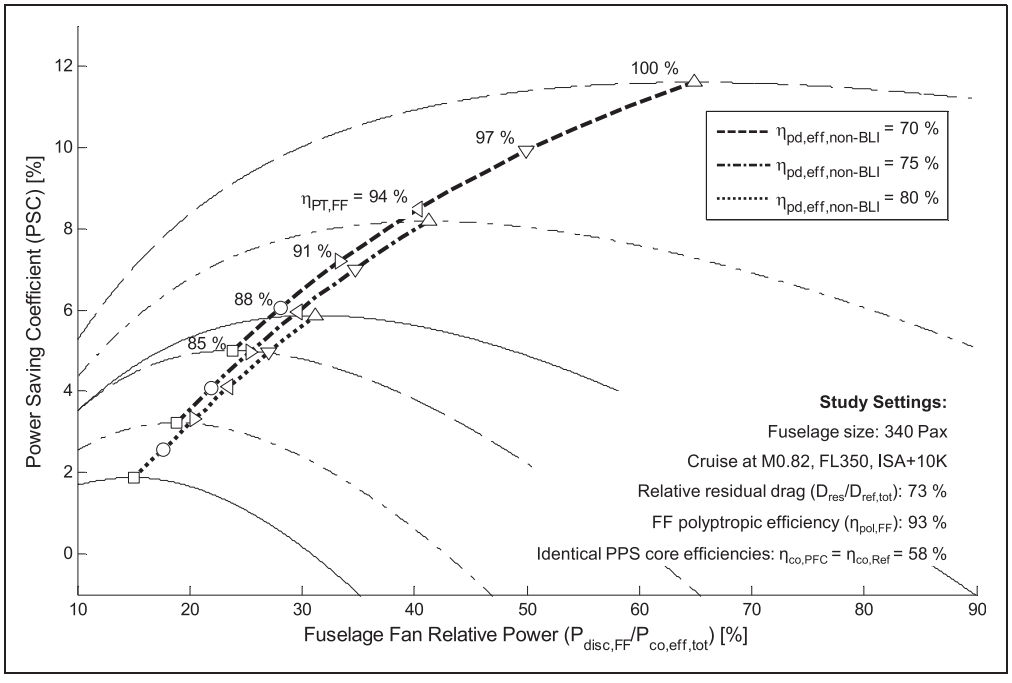

Figure 8. Identification of optimum PSC and corresponding FF relative powers for various power train and non-BLI propulsive device efficiencies.

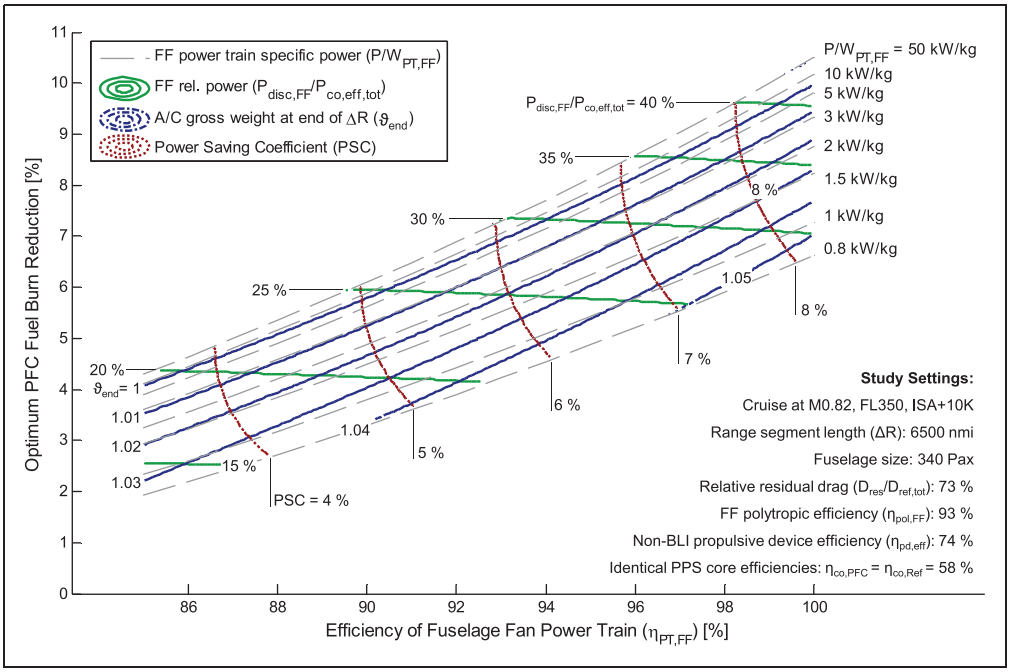

Figure 9. System weight impact on optimum PFC fuel savings and corresponding FF relative power levels.

corresponding maximum *PSC* trends displayed in Figure 8, taking into account the range-specific efficiency amplification effect due to the Breguet–Coffin equation (cf. Figure 3). With the $\vartheta_{end} = 1$ line indicating the maximum fuel saving curve and corresponding optimum PFC design for the given transport task without PFC empty weight penalty, the fuel impact with increasing PFC empty weight penalty ($\vartheta_{end} > 1$) is obvious. The penalty in PFC fuel savings ranges between approximately 0.5% and 0.7% per percent increase in ϑ_{end} with a slightly progressive trend with growing ϑ_{end}. If propulsion installation weight penalties are neglected, i.e. $\Delta m_{OWE,Res} = 0$, Figure 9 provides the direct translation of $P/W_{PT,FF}$ to PFC fuel savings. As can be seen from the figure, PFC empty weight neutrality, i.e. $\vartheta_{end} = 1$, is reached for $P/W_{PT,FF}$ values between approximately 7 kW/kg and 9 kW/kg with the higher *PSC* lowering the $P/W_{PT,FF}$ threshold value. For decreasing $P/W_{PT,FF}$, the PFC fuel penalty is increasing non-linearly. Assuming $P/W_{PT,FF} =$ 2 kW/kg for the turbo-electric FF transmission scenario featuring $\eta_{PT,FF} = 91\%$, the optimum PFC fuel savings yield 5.2%. With an assumed $P/W_{PT,FF} =$ 10 kW/kg for the mechanical FF transmission scenario featuring $\eta_{PT,FF} = 98\%$, the optimum PFC fuel savings are 9.1% which is in good agreement with the results previously obtained from the DisPURSAL project.[15] If the reference aircraft relative residual drag $D_{Ref,res}/D_{Ref,tot}$ is reduced from the baseline value of 73% by relative 10%, e.g. through significantly enhanced wing flow laminarity, PFC fuel savings relative to the non-BLI reference aircraft increase to 5.7% in the turbo-electric scenario, and 9.9% in the mechanical case.

Conclusion and further work

The paper provides a rigorous methodical approach for the evaluation of the power-saving potentials of PFC aircraft configurations. Analytical formulation for the *PSC* metric was introduced and the classic Breguet–Coffin range equation was extended for the analytical assessment of BLI aircraft. The analytical formulation was applied to the identification of optimum PFC power savings together with CFD numerical results of refined and optimised 2D aero-shapings of the bare PFC configuration, i.e. fuselage body including the aft–fuselage BLI propulsive device, obtained during the DisPURSAL and CENTRELINE projects. A common heuristic for the BLI efficiency factor was derived from the best aero-shaping cases of both projects. Using the derived PFC design and performance heuristic, maximum power savings and corresponding optimum PFC design settings were parametrically analysed and discussed with regard to relevant power train configurations. It was found that the optimum PFC aircraft design is strongly dependent on the efficiency levels of the transmission system and the effective efficiency levels of the involved non-BLI propulsive devices.

Improving transmission system efficiency increases the achievable power savings, and, shifts the optimum ratio of FF to total fan power to higher values. If the effective propulsive device efficiency of the reference aircraft and PFC main engines increases, the attainable PFC power savings are reduced and optimum relative FF power levels decrease. In a direct comparison between typical settings for mechanical and conventionally conducting turbo-electric scenarios

for the power transmission from the core engine exit to the FF, the mechanical option features higher fuel burn reduction potentials than turbo-electric transmission, if FF aero-structural integration can be mastered. The analysis results confirm the necessity for a highly optimised PFC aero-shaping, an ultra-efficient FF power train and minimum installation weight penalty, in order to achieve high fuel burn savings for a PFC aircraft configuration.

The presented optimality analyses focused explicitly on a 340 passenger medium-to-long range aircraft application with design cruise conditions at M0.82, FL350, ISA + 10 K based on 2D axisymmetric aero-shaping results. However, by parametric extension of the developed BLI efficiency factor heuristic, the methodology introduced in the paper directly enables the PFC power savings evaluation for aircraft of different sizes under 3D aero-shaping paradigms. This also includes the investigation of alternative flight techniques.

Recommended future work involves a more detailed resolution of aerodynamic interference effects between the bare PFC configuration and the adjacent aircraft components and the analysis of the 3D aero-shaping implications on the power-saving potentials of PFC aircraft configurations. As part of the presented study, possible synergy potentials with additional annexed technologies were highlighted. For this purpose, future work should consider PFC technology as a key item within an overall technology package for ultra-efficient transport aircraft and explore technological synergy potentials in a systematic way. This should include ultra-efficient wing aerodynamics including hybrid and natural flow laminarity and self-trimming wing properties, the combination with radically advanced aero engine cycle technologies, as well as the application of alternative energy options such as liquid hydrogen fuel.

Acknowledgements

The authors convey their gratitude to Richard Grenon and Jean-Luc Godard from ONERA – The French Aerospace Lab for kindly providing the CFD results obtained from the DisPURSAL design studies. Arne Seitz would like to thank Markus Nickl for fruitful discussions on the effective core engine excess power parameter, and, Mirko Hornung for valuable feedback and advice.

Declaration of Conflicting Interests

The author(s) declared no potential conflicts of interest with respect to the research, authorship, and/or publication of this article.

Funding

The author(s) disclosed receipt of the following financial support for the research, authorship, and/or publication of this article: The CENTRELINE project has received funding from the European Union's Horizon 2020 research and innovation programme under Grant Agreement No. 723242. The DisPURSAL project has received funding from the European Union's Seventh Framework Programme (FP7) under Grant Agreement No. 323013.

ORCID iD

Arne Seitz https://orcid.org/0000-0002-8842-2755

Notes

a. In case of separate nozzles for the core and bypass flows in a turbofan engine, P_{jet} equals the sum of core and bypass jet powers, $P_{jet,co}$ and $P_{jet,bp}$.
b. In case of turbofan engines, this is the outer fan.
c. Please note: At steady-level flight condition, this implies identical instantaneous gross weights of aircraft, the BLI PFC and the non-BLI reference. c. In strong yaw, a growing interference between the aft–fuselage section and the propulsive jet flow of the main engines is expected.
d. For the non-BLI power plants installed on the reference and PFC aircraft, identical $\eta_{pd,eff}$ are assumed. This means significantly smaller fan diameters for the PFC main engines and correspondingly reduced nacelle wetted areas.
e. Note: The effective propulsive device efficiency for the non-BLI power plants $\eta_{pd,eff,non\text{-}BLI}$ includes the mechanical efficiencies of the LP spool and the fan drive gear box which feature a combined efficiency of approximately 99%.

References

1. Smith AMO and Roberts HE. The jet airplane utilizing boundary layer air for propulsion. *J Aero Sci* 1947; 14: 97–109, 128.
2. Goldschmied FR. A theoretical aerodynamic analysis of a boundary layer controlled airship hull. Goodyear Aircraft Report GER-6251, 1954.
3. Smith LH. Wake ingestion propulsion benefit. *J Propul Power* 1993; 9: 74–82.
4. Drela M. Power balance in aerodynamic flows. *AIAA J* 2009; 47: 1761–1771.
5. Cerreta PA. Wind-tunnel investigation of the drag of a proposed boundary-layer controlled airship. David Taylor Model Basin Aero Report 914, 1957.
6. Atinault O, et al. Numerical and Experimental Aerodynamic Investigations of BLI for Improving propulsion efficiency of future air transport. In: 31st AIAA Applied Aerodynamics Conference, San Diego, CA, 24–27 June, 2013.
7. Lv P, Rao AG, Ragni D, et al. Performance analysis of boundary layer ingestion for aircraft design. *J Aircraft* 2016; 53: 1517–1527.
8. Uranga A, et al. Preliminary experimental assessment of the boundary layer ingestion benefit for the D8 aircraft, AIAA 2014-0906, AIAA SciTech 52nd, Aerospace Sciences Meeting. National Harbor, Maryland, USA, 13–17 January, 2014.
9. Steiner H-J, Seitz A, Wieczorek K, et al. Multi-disciplinary design and feasibility study of distributed propulsion systems. In: 28th International Congress of the Aeronautical Sciences, Brisbane, Australia, 23–28 September, 2012.
10. Heppner FAM. Improvements relating to jet-propelled aircraft. GB Patent GB577950, issued 1941.

11. Bolonkin A. A high efficiency fuselage propeller ('Fusefan') for subsonic aircraft. In World Aviation Conference, San Francisco, 1999.
12. Stückl S, van Toor J and Lobentanzer H. VoltAir – the all electric propulsion concept platform – a vision for atmospheric friendly flight. In 28th International Congress of the Aeronautical Sciences (ICAS), Brisbane, Australia, 23–28 September, 2012.
13. Bradley MK and Droney CK. Subsonic ultra green aircraft research phase II: N+4 advanced concept development. NASA/CR-2012-217556, Langley Research Center Prepared for Langley Research Center, Hampton, Virginia, May 2012.
14. Welstead L and Felder J. Conceptual design of a single-aisle turboelectric commercial transport with fuselage boundary layer ingestion. AIAA-2016-1027, 54th AIAA Aerospace Sciences Meeting (SciTech), San Diego, CA, 4–8 January, 2016.
15. Isikveren AT, Seitz A, Bijewitz J, et al. Distributed propulsion and ultra-high bypass rotor study at aircraft level. *Aeronaut J* 2015; 119: 1327–1376.
16. Seitz A, Peter F, Bijewitz J, et al. Concept validation study for fuselage wake-filling propulsion integration. Paper-ID 0382, 31st International Congress of the Aeronautical Sciences (ICAS), Belo Horizonte, Brazil, 09–14 September, 2018.
17. Gray JS and Martins JRRA. Coupled aeropropulsive design optimization of a boundary layer ingestion propulsor. *Aeronaut J* 2018; 123: 121–137.
18. Habermann AL, Bijewitz J, Seitz A, et al. Performance bookkeeping for aircraft configurations with fuselage wake-filling propulsion integration. *CEAS Aeronaut J*. Epub ahead of print 2 December 2019. DOI: 10.1007/s13272-019-00434-w.
19. MIDAP Study Group. Guide to in-flight thrust measurement of turbojets and fan engines. AGARDograph No. 237, 1979.
20. Seitz A, Schmitz O, Isikveren AT, et al. Electrically powered propulsion: comparison and contrast to gas turbines. Paper No. 1358, 61. Deutscher Luft- und Raumfahrtkongress 2012, Berlin, Germany, 10–12 September, 2012.
21. Kurzke J. GasTurb 11 – design and off-design performance of gas turbines. Software Manual, 2007.
22. Cambier L, Heib S and Plot S. The ONERA elsA CFD software: input from research and feedback from industry. *Mech Indust J* 2013; 14: 159–174.
23. Glauert H. *Airplane propellers – aerodynamic theory*. Volume 4. s.l. Durand Editor. New York: Dover Publications.
24. van Leer B. Towards the ultimate conservative difference scheme, V. A second-order sequel to Godunov's method. *J Computat Phys* 1979; 32: 101–136.
25. Leonard BP. A stable and accurate convective modelling procedure based on quadratic upstream interpolation. *Comput Methods Appl Mech Eng* 1979; 19: 59–98.
26. Kaiser S, Donnerhack S, Lundbladh A, et al. Composite cycle engine concept with hectopressure ratio. *AIAA J Propul Power* 2016; 32: 1413–1421.
27. Seitz A, Nickl M, Stroh A, et al. Conceptual study of a mechanically integrated parallel hybrid electric turbofan. *Proc IMechE Part G: Journal of Aerospace Engineering* 2018; 232: 2688–2712.
28. Bijewitz J, Seitz A and Hornung M. Extended design studies for a mechanically driven propulsive fuselage aircraft concept. AIAA 2018-0408, Aerospace Sciences Meeting (AIAA SciTech Forum), Kissimmee, FL, 8–12 January, 2018.
29. Bijewitz J, Seitz A and Hornung M. Power plant predesign exploration for a turbo-electric propulsive fuselage concept. AIAA 2018-4402, AIAA Propulsion and Power Forum 2018, Cincinnati, OH, 9–11 July 2018.
30. Samuelsson S, Petit O, Merkler R, et al. Adaption of a turbofan engine for high power offtakes for a turboelectric propulsive fuselage concept. ISABE-2019-24215, 24th ISABE Conference, Canberra, Australia, 22–27 September, 2019.
31. Trapani M, Pleißner M, Isikveren AT, et al. Preliminary investigation of a self-trimming non-planar wing using adaptive utilities. Paper No. 1316, 61. Deutscher Luft- und Raumfahrtkongress 2012, Berlin, 10–12 September 2012.
32. Gunn EJ and Hall CA. Aerodynamics of boundary layer ingesting fans. GT2014-26142, ASME Turbo Expo, Düsseldorf, Germany, 16–20 June 2014.
33. Castillo Pardo A and Hall CA. Aerodynamics of boundary layer ingesting fuselage fans. ISABE-2019-24162, 24th ISABE Conference, Canberra, Australia, 22–27 September, 2019.
34. Seitz A, Bijewitz J, Kaiser S, et al. Conceptual investigation of a propulsive fuselage aircraft layout. *Aircraft Eng Aerospace Technol J* 2014; 86: 464–472.
35. Seitz A, Isikveren AT, Bijewitz J, et al. Summary of distributed propulsion and ultra-high by-pass rotor study at aircraft level. Paper ID paper: 3E-1. In: Aviation in Europe – Innovation for Growth. Proceedings from the Seventh European Aeronautics Days, London, 20–22 October 2015, 2017.
36. Bijewitz J, Seitz A and Hornung M. Multi-disciplinary design investigation of propulsive fuselage aircraft concepts. *Aircraft Eng Aerosp Technol J* 2016; 88: 257–267.
37. Peter F, Bijewitz J, Habermann AL, et al. Definition of the CENTRELINE reference aircraft and power plant systems. Presentation at 9th International EASN Conference, Athens, Greece, 3–6 September, 2019.
38. Rogalsky T and Derksen RW. Optimum aerofoil parameterization for aerodynamic design. *Comput Aided Optimum Design Eng* 2009; XI: 197–206.
39. Shields MD and Zhang J. The generalization of Latin hypercube sampling. *Reliability Eng Syst Safety* 2016; 184: 96–108.
40. Chang CC and Lin CJ. LIBSVM: a Library for support vector machines. *ACM Trans Intell Syst Technol* 2011; 2: Article 27.

Appendix

Notation

A	area (m^2)
D	drag (N)
F	force; thrust (N)
FHV	lower fuel heating value
f_η	efficiency factor (–)
g	standard gravity (m/s^2)
h	enthalpy (m^2/s^2)

L	lift (N)
M	Mach number (–)
m	mass (kg)
$\dot{m}$	mass flow (kg/s)
NPF	net propulsive force (N)
P	power (W)
p	pressure (kg/m^3)
P/W	power-to-weight ratio (kW/kg)
R	range (m)
V	velocity (m/s)
ε	energy source (J/m^3)
η	efficiency (–)
ϑ	aircraft gross weight ratio (–)

Subscripts

0	freestream
2	fan front face
A/C	aircraft
amb	ambient
bp	bypass
co	core
disc	disc
eff	effective
emp	empennage
f	fuel
fus	fuselage
id	ideal
int	interference
is	isentropic
jet	jet
main	Main
mech	mechanical
misc	miscellaneous
nac	Nacelle
o	outer
ov	overall
pd	propulsive device
pol	polytropic
pr	propulsive
pyl	pylon
res	residual
s	static
sht	shaft
supply	supply
thrust	thrust
tot	total
tr	transmission
wing	wing
A	axial
ACC	accessories
BTE	bare turbo engine
CE	core exit
F	fan
FF	fuselage fan
Gen	generator
LP	low pressure
Mot	motor
N	net
PG	propulsion group
PL	payload
PT	power train
Ref	reference (aircraft)
TE	turbo-electric
TM	transmission
AOA	angle of attack
LPT	low pressure turbine
PMAD	power management and distribution system